Nanoscale

PAPER

View Article Online
View Journal | View Issue

Cite this: *Nanoscale*, 2016, **8**, 18412

Investigating the all-solid-state batteries based on lithium garnets and a high potential cathode – $LiMn_{1.5}Ni_{0.5}O_4$†

Christian Hänsel, Semih Afyon* and Jennifer L. M. Rupp*

Received 2nd September 2016,
Accepted 29th September 2016

DOI: 10.1039/c6nr06955j

www.rsc.org/nanoscale

All-solid-state Li-ion batteries based on lithium garnets give new prospects for safer battery operations avoiding liquids, and could enable the integration of high energy density electrode materials. Herein, we critically investigate the structural and chemical stability of the high voltage cathode material, $LiMn_{1.5}Ni_{0.5}O_4$, based on the solid lithium garnet electrolyte LLZO (c-$Li_{6.4}Ga_{0.2}La_3Zr_2O_{12}$) for all-solid Li-ion batteries. We manufacture battery cells based on nano-grained synthesized LLZO and composite cathodes ($LiMn_{1.5}Ni_{0.5}O_4$/LLZO/C) fabricated *via* direct slurry casting of the cathode material and additives on sintered LLZO pellets against metallic Li anodes. The galvanostatic tests of such all-solid-state batteries up to 4.9 V at 95 °C reveal the incompatibility of the solid electrolyte and the cathode material under given conditions. Post-mortem analyses of the all-solid-state batteries demonstrate the formation of new inactive phases at the LLZO/$LiMn_{1.5}Ni_{0.5}O_4$ interfacial region through an irreversible reaction starting at ~3.8 V during charging. The discovered limited chemical stability under the investigated conditions raises the question if LLZO could be a promising solid-electrolyte for future all-solid-state Li-ion batteries especially at higher operation potentials and demanding operation conditions.

Introduction

Electrical energy storage is one of the most essential needs of the 21st century. The rapid increase of portable electronic devices and electric mobility demands rechargeable batteries of light weight, long cycle life, variable charge/discharge rates and low cost. Due to the lowest negative potential of the Li^+/Li redox couple (−3.04 V *vs.* standard hydrogen electrode (SHE)) among metals and the light weight of lithium (M = 6.4 g mol^{-1} and ρ = 0.53 g cm^{-3}), Li-ion batteries (LIBs) play the key role in energy storage.[1–3] However, conventional LIBs based on a liquid electrolyte possess significant safety issues such as chemical stability, flammability and leakage. Solid electrolytes could overcome these problems since they offer improved chemical and thermal stability and leakage-free properties. Due to their wide stable potential window and chemical stability, solid electrolytes could be expected to enable the use of metallic lithium and high capacity electrode materials, such as vanadate[4] and sulphur[5,6] based ones, which show long term stability issues in combination with liquid electrolytes. In addition, solid electrolytes may allow improved designs of new and lighter casings. Combining all these advantages, solid electrolytes may be the key to future safe and high energy density Li-ion batteries.

A large number of inorganic solid Li-ion electrolytes have been investigated to date showing different chemical stabilities at the electrolyte/electrode interface and ionic conductivities.[7,8] Among various types of inorganic solid electrolytes, the garnet-type $Li_7La_3Zr_2O_{12}$ (LLZO) electrolyte, first reported by Murugan *et al.*[9] attracted much attention due to its high Li-ion conductivity (~10^{-4} S cm^{-1} at RT) and its good chemical stability against metallic lithium. The garnet-type $Li_7La_3Zr_2O_{12}$ electrolyte has two crystal structures, namely, a high ionic conducting cubic structure,[9] that could be only stabilized by Li or La site doping, and a low conducting (~10^{-6} S cm^{-1} at RT) tetragonal structure.[10,11] Synthesis of pure high conducting cubic LLZO and stabilization over the low conducting tetragonal LLZO are still challenging, and reports investigating the stabilization, synthesis and processing of the cubic phase can be found in the literature.[12–22] The stabilization of the cubic phase not only requires extrinsic doping but also requires high synthesis and processing temperatures to synthesize highly conducting Li-electrolyte ceramics. Conventionally, if classic routes (*e.g.* solid state powder synthesis) are followed, high densities can be achieved for ceramics, but at the same time the elevated Li-losses at high annealing temperatures have to be kept to a minimum to assure fast Li transport. This also

ETH Zurich, Department of Materials, CH-8093 Zurich, Switzerland.
E-mail: semih.afyon@alumni.ethz.ch, jennifer.rupp@mat.ethz.ch

†Electronic supplementary information (ESI) available. See DOI: 10.1039/c6nr06955j

leads to large micron sized particles and grains (*ca.* 20–30 μm) that are unfavorable for the construction of all-solid-state batteries based on LLZO inorganic solid electrolytes as the interconnectivity at the electrode–electrolyte interfaces is reduced. Very recently, the first successful stabilization of the cubic phase through post-Ga^{3+} doping *via* a low temperature synthesis route described by Afyon *et al.* was reported,[23] which resulted in nanoparticles of purely cubic $Li_{6.4}Ga_{0.2}La_3Zr_2O_{12}$ of 200–300 nm in average, while maintaining the structural properties of Li in the ceramic densification synthesis of the electrolyte pellets.

This method decreases the Li-loss during synthesis and yields the desired single phase $Li_{6.4}Ga_{0.2}La_3Zr_2O_{12}$ nanoparticles. Therefore, it could be well adapted and form the basis to assemble composite electrodes with fast Li^+ diffusion solid electrode–electrolyte interfaces and all-solid-state Li-ion batteries based on LLZO garnets in future. The research in the field of LLZO is going on for years and many different synthesis and doping strategies have been published and summarized in the literature.[11] However, the assembly and electrochemical testing of all-solid-state batteries by actually utilizing LLZO electrolytes in combination with various electrode materials require more attention.

Only a few reports have investigated the fabrication, microstructure and electrochemical characteristics of electrode materials for all-solid-state batteries based on LLZO solid electrolytes so far, which we summarized in a recent publication.[24] Here, the best investigated electrode material for assembly with LLZO electrolytes is the well-known cathode material $LiCoO_2$.[25–30] In these reports the cathode material $LiCoO_2$ was predominantly assembled by co-sintering of the electrode and electrolyte powder or by depositions as thin films on solid state LLZO pellets. However, promising electrochemical battery performances have so far only been achieved for $LiCoO_2$ cathodes in the form of thin films, *e.g.* deposited *via* vacuum techniques like pulsed laser deposition (PLD).[26,27] Computational studies based on density functional theory (DFT) by the Ceder group[31] and Zhu *et al.*[32] investigated the stability of LLZO in combination with various cathode materials such as $LiCoO_2$, $LiFePO_4$ and $LiMnO_2$. The theoretical studies show calculated intrinsic stability windows of LLZO and cathodes and predict their interface reactions. Despite the theoretical effort it remains still unclear how the all-solid-state battery assemblies based on established electrodes perform and which interfacial reactions and stabilities are found under real battery operation conditions for LLZO. This is surprising since several state-of-the-art cathode materials are tested in classic polymeric/liquid electrolyte battery assemblies, but have not been applied to LLZO solid state battery cells yet.

An interesting alternative to conventionally used cathode materials is the high operation voltage cathode material $LiMn_{1.5}Ni_{0.5}O_4$.[33–36] Due to its high energy density of over 600 W h kg^{-1} and high operation voltage of ~4.7 V, $LiMn_{1.5}Ni_{0.5}O_4$ is an attractive candidate for next generation Li-ion batteries[36] but has not been tested towards LLZO electrolytes in all-solid-state batteries yet. This is surprising, as it may even have higher implications on solid state batteries when successfully integrated with solid state electrolytes due to its capacity fading resulting from the dissolution of transition metals into the classic liquid electrolytes.[33,37] Besides, high charging potentials above ~4.5 V could lead to the decomposition of standard carbonate-based liquid electrolytes and the lack of stable solid/electrolyte interphase (SEI). Integration of $LiMn_{1.5}Ni_{0.5}O_4$ in all solid-state batteries based on LLZO garnets could address these problems, since solid electrolytes could prevent the dissolution of manganese and offer wider operation windows. On top the higher operation voltage of $LiMn_{1.5}Ni_{0.5}O_4$ (4.7 V) compared to $LiCoO_2$ (3.8 V)[3] would theoretically enable higher power outputs at lower currents when successfully combined with a solid state electrolyte. The lowered operation currents would be highly advantageous for all-solid-state batteries where the transportation of charge carriers is conventionally more limited compared to liquid based batteries due to the generally low ionic conduction of the solid electrolyte. Thus, $LiMn_{1.5}Ni_{0.5}O_4$ is an interesting cathode material to investigate the stability and electrochemical performance towards LLZO solid state electrolytes for all-solid-state batteries and is the subject of this first investigation utilizing LLZO as the solid electrolyte.

In this work, we report on the processing and stability of all-solid-sate Li-ion batteries based on the cathode material $LiMn_{1.5}Ni_{0.5}O_4$ combined with a low temperature synthesized cubic $Li_{6.4}Ga_{0.2}La_3Zr_2O_{12}$ garnet-type electrolyte. Batteries are constructed *via* direct slurry casting of the cathode material and additives on c-$Li_{6.4}Ga_{0.2}La_3Zr_2O_{12}$ pellets and using metallic Li as the anode. Testing of all-solid-state batteries at high operation voltages of up to 4.9 V at 95 °C gives indication of the chemical compatibility of LLZO in combination with $LiMn_{1.5}Ni_{0.5}O_4$ and the battery performance of high voltage all-solid state Li-ion batteries. Finally, we conclude on the suitability and operation of $LiMn_{1.5}Ni_{0.5}O_4$ cathodes for LLZO all-solid Li-ion batteries.

Experimental

Synthesis, powder and pellet processing of the c-$Li_{6.4}Ga_{0.2}La_3Zr_2O_{12}$ solid electrolyte

For the synthesis of cubic $Li_{6.4}Ga_{0.2}La_3Zr_2O_{12}$, stoichiometric amounts of $LiNO_3$ (99% Alfa Aesar), $Al(NO_3)_3{\cdot}9H_2O$ (99%, Fluka Chemika), $La(NO_3)_3{\cdot}6(H_2O)$ (99.9%, Alfa Aesar), and zirconium(IV) acetylacetonate (98% abcr) were dissolved in a water/ethanol mixture at 70 °C; Ga_2O_3 was used as the Ga source in a stoichiometric amount and was also added to this solution. To avoid possible Li-loss during calcination and sintering, the lithium precursor was taken in a slight excess of 10 wt% relative to the other precursor. The solvent was left to evaporate overnight at 95 °C to obtain a xerogel. The gel was ground in a mortar and calcined in a vertical tube furnace at 650 °C at a heating/cooling rate of 5 °C min^{-1} for 15 h in a MgO crucible under a constant synthetic airflow.

The calcined powder was ground and pressed pellets (of 1–2 mm thickness and 13 mm diameter) were prepared by uniaxial pressing at 35 kN followed by cold isostatic pressing (Weber Presse, Germany) at 1000 kN. The powder pellets were polished with P1200 sand paper to remove surface impurities and then sintered at temperatures between 950 and 1000 °C in a horizontal tube furnace at a heating/cooling rate of 5 °C min^{-1} for 10 h under a constant O_2 flow and covered with the parent powder to avoid Li-losses and Mg contamination from the MgO crucibles. Pellets sintered at 950 °C had relative densities of ~78% and pellets sintered at 1000 °C showed increased densities of ~84%.

Throughout the study, all sample powders and sintered pellets were kept under an inert N_2 atmosphere or stored in an argon filled glove box to minimize the exposure to humidity.

Interface-engineering of the solid electrolyte

For the preparation of a porous pellet surface a LLZO/starch slurry was prepared by mixing $Li_{6.4}Ga_{0.2}La_3Zr_2O_{12}$ and starch (Patissier, Migros) in the weight ratio 3 : 1. 100 mg of the mixture were dispersed in 2 ml of THF/toluene (4 : 1 vol. ratio) in an ultrasonic bath for 1 h. LLZO pellets were abraded with sandpaper (P400/P600) to the desired thickness and 3 droplets of the LLZO/starch slurry were dropped onto the pellet. The solvent was left to evaporate at room temperature before the procedure was repeated two more times to guarantee a uniform coverage of the pellet. The modified pellets were then dried in a Schlenk flask under a vacuum at 100 °C for 1 h. Then the pellets were sintered at 950 °C in a horizontal tube furnace for 10 hours at a heating rate of 1 °C min^{-1} under a constant O_2flow and covered with LLZO powder to avoid Li-losses and Mg contamination from the MgO crucible.

All-solid-state battery assembly and electrochemical tests

For the assembly of all-solid-state batteries dense $Li_{6.4}Ga_{0.2}La_3Zr_2O_{12}$ pellets were abraded with sandpaper (P400/P1200) to the desired thickness. Batteries were assembled with $LiMn_{1.5}Ni_{0.5}O_4$ as the positive electrode and the Li metal as the negative electrode with non-modified or interface-engineered solid electrolyte c-$Li_{6.4}Ga_{0.2}La_3Zr_2O_{12}$ pellets respectively *via* slurry casting deposition, see Fig. 1(a). An electrode slurry was prepared by first mixing $Li_{6.4}Ga_{0.2}La_3Zr_2O_{12}$ powder, $LiMn_{1.5}Ni_{0.5}O_4$ (Life Power®, Johnson Matthey) conductive carbon (Super P® Li Timcal), and polyvinylidene fluoride (PVDF, Sigma-Aldrich) binder in the weight ratio 3 : 5 : 1 : 1. 75 mg of the powder mixture was than dissolved in 1 ml THF/toluene (4 : 1 vol. ratio) and ultrasonicated for 1 h to ensure homogeneous mixing of the components. 6–7 droplets of the electrode slurry were dropped on the pellet with a Pasteur pipette. The solvent was left to evaporate at room temperature before the pellet was dried in a Schlenk flask at 100 °C under vacuum for 1 h. After cooling to room temperature the pellet was wrapped into an Al-foil to prevent sticking of the cathode to the protection rubbers which are needed for isostatic pressing of the pellet at 1000 kN. After pressing, a thin Pt layer (14 nm) was sputtered on the cathode side (sputtering machine). Swagelok-cells were assembled in an Ar-filled glovebox with the Li-metal as the

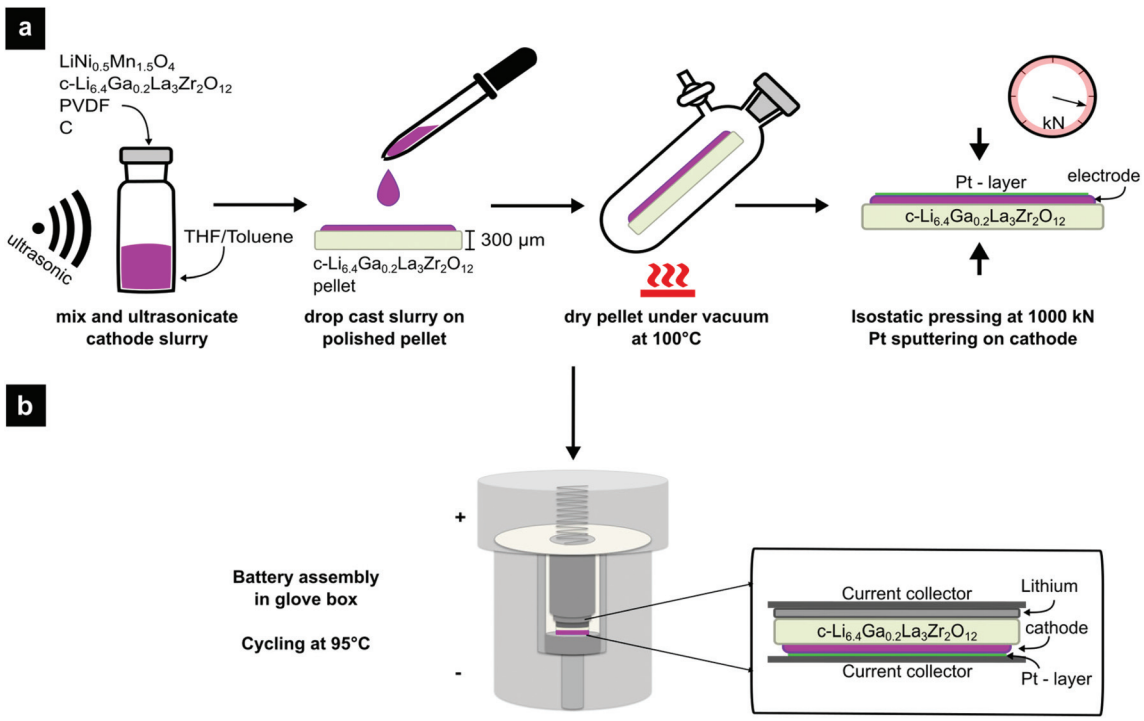

Fig. 1 Schematic representation (a) of the cathode slurry deposition and (b) all-solid-state battery assembly based on the c-$Li_{6.4}Ga_{0.2}La_3Zr_2O_{12}$ electrolyte with the $LiMn_{1.5}Ni_{0.5}O_4$ composite and Li-metal electrodes.

anode prepared from a 0.75 mm thick Al foil (Alfa Aesar), see Fig. 1(b).

For battery performance tests non-modified and interface-engineered all-solid-state batteries were cycled in a galvanostatic mode at 95 °C between 3.0 V and 4.9 V at a current rate of 2 A kg^{-1}.

For the AC measurements, the pellets were polished with sand paper and Pt was sputtered on both sides. Pt wires were glued on both sides of the pellet with a ceramic binder (Thermokit Roth). Then, the pellet was painted with Pt paste (C 3605 S, Heraeus) from both sides and dried under vacuum. The electrochemical impedance spectroscopy (EIS) measurement was performed with a Gamry Reference 600 potentiostat/galvanostat/ZRA (zero resistance ammeter) in the frequency range of 1 MHz to 0.1 Hz with an alternating voltage of 10 mV and the spectra were analyzed using the ZView software.[38]

Chemical and structural characterization

Powder X-ray diffraction (XRD) patterns of the powder samples were obtained using a STOE Stadi P diffractometer equipped with a germanium monochromator and $CuK_{\alpha1}$ radiation operated at 36 mA and 35 kV.

Scanning electron microscopy (SEM) analysis of the samples was carried out using a Zeiss Gemini 1530.

Energy-dispersive X-ray spectroscopy (EDX) measurements were performed using an INCA EDS X-ray spectrometer.

Results and discussion

The synthesis of c-$Li_{6.4}Ga_{0.2}La_3Zr_2O_{12}$ nanopowders is based on a modified sol–gel route introduced by Afyon *et al.*[23] (note that here for this synthesis, Ga_2O_3 was added from the beginning to simplify the synthesis route). For the assembly of all-solid-state batteries, calcined LLZO powder was pressed and sintered to c-$Li_{6.4}Ga_{0.2}La_3Zr_2O_{12}$ pellets, see ESI Fig. 1a–d.† The ionic conductivity of c-$Li_{6.4}Ga_{0.2}La_3Zr_2O_{12}$ pellets was measured by AC impedance spectroscopy and is comparable to earlier reports,[23,24] see the ESI for details (ESI Fig. 2†).

After the successful synthesis and processing of c-$Li_{6.4}Ga_{0.2}La_3Zr_2O_{12}$ pellets, these were used to build all-solid-state batteries: for this, the composite cathode material consisting of $LiMn_{1.5}Ni_{0.5}O_4$, c-$Li_{6.4}Ga_{0.2}La_3Zr_2O_{12}$, Super P carbon and PVDF is directly casted on the sintered pellets as a slurry, see Fig. 1a. Eventually, the electrodes were isostatically pressed at 1000 kN on the solid electrolyte in order to obtain a good integration. Scanning electron microscopy (SEM) micrographs of the pellet cross-section after pressing are displayed in Fig. 2a and b, showing a 450 μm thick and dense solid electrolyte pellet and the ~15–20 μm thin composite cathode layer. We interpret the micrograph as a well embedded electrode structure towards the solid electrolyte. No delamination or void formation is visible at the cathode–electrolyte interface, Fig. 2b. Compared to the SEM micrograph of the cross-section of a non-pressed pellet, see ESI Fig. 3,† the pressing not only leads to a good integration of the two layers but also minimizes the thickness of the electrode. In the next step, we use the successfully assembled solid electrolyte c-$Li_{6.4}Ga_{0.2}La_3Zr_2O_{12}$ and cathode $LiMn_{1.5}Ni_{0.5}O_4$ to construct all-solid-state battery cells integrating a Li metal anode and current collectors. To ensure a good contact between the electrode and the current collector a thin Pt layer was also deposited *via* sputtering, see Fig. 1a and b. The cells are then tested in a galvanostatic mode at a rate of 2 A kg^{-1} between 4.9 V and 3.0 V. However, even though all-solid-state batteries constructed in such a way have stable and reproducible open circuit voltages (OCV) of ~3.0 V and the first charge process can be successfully initiated, an irreversible reaction is found at ~3.8 V leading to a potential drop and to an irreversible reaction and continuous decomposition at lower potentials, see Fig. 2c. This process is not reversible and detrimental to the cells, as they cannot be discharged in subsequent cycles. In order to further investigate this finding and understand if any interfacial characteristics or processing parameters contribute to the irreversible reaction, all-solid-state batteries are constructed based on c-$Li_{6.4}Ga_{0.2}La_3Zr_2O_{12}$ pellets of different relative densities and surface structures and are tested in the same galvanostatic mode, see ESI Fig. 4.†

For different surface structures, thin and porous LLZO interlayers are manufactured in between the LLZO electrolyte and the $LiMn_{1.5}Ni_{0.5}O_4$ electrode layer, as described by Van den Broek *et al.*[24] The relative pellet density could be controlled by adjusting the sintering temperature.

Interestingly, all different batteries show a very similar galvanostatic charge profile and a potential drop after reaching a working potential of ~3.8 V regardless of the pellet density or the interface design, see ESI Fig. 4.† The consistency observed in the cells of different morphologies and surface structures shows that the pellet density and interface design have no influence on the battery performance in this case. But, it is rather an indication of an irreversible reaction between the cathode material $LiMn_{1.5}Ni_{0.5}O_4$ and the solid electrolyte c-$Li_{6.4}Ga_{0.2}La_3Zr_2O_{12}$ under given operation conditions. Theoretical investigation by Ceder *et al.*[31] using density functional theory (DFT) predicted a possible stability limit for LLZO at high operation voltages in combination with various cathode materials (*e.g.* $LiCoO_2$, $LiFePO_4$, $LiMnO_2$) which is in line with our findings here. Ceder *et al.*[31] searched for the reactions between the electrolyte and the cathode which are driven by the given lithium chemical potential that depends on the state of charge. In their work the authors calculated the intrinsic stability window for LLZO in combination with the cathode material. The potential limit of ~3.8 postulated by Ceder *et al.*[31] where the driving force for the decomposition of LLZO is the highest at the partially charged state of the cathode, also matches very well with our experimental observations reported here and can be confirmed for the newly tested cathode $LiMn_{1.5}Ni_{0.5}O_4$, see Fig. 2c.

In order to further investigate the possible incompatibility between the cathode and the solid electrolyte, X-ray powder diffraction patterns of the composite electrode before and after the battery operation were collected. The XRD powder patterns

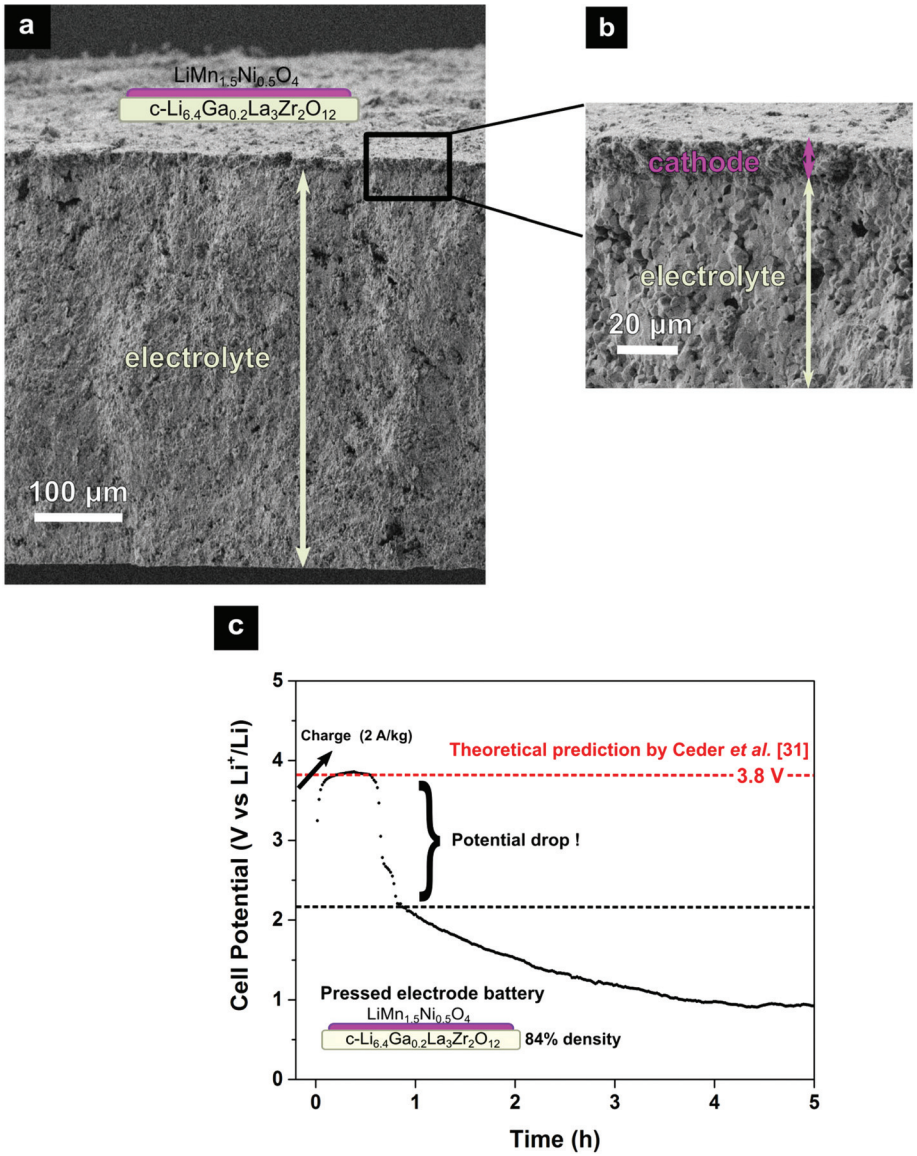

Fig. 2 (a) Scanning electron microscopy (SEM) image of the cross section of a pressed c-$Li_{6.4}Ga_{0.2}La_3Zr_2O_{12}$ pellet (relative density 84%) with the $LiMn_{1.5}Ni_{0.5}O_4$ composite electrode and (b) zoomed-in view of the interface region of the electrolyte and electrode. (c) Cell potential *versus* time for the first charging process (2A kg^{-1}) of an all-solid-state battery based on c-$Li_{6.4}Ga_{0.2}La_3Zr_2O_{12}$ with $LiMn_{1.5}Ni_{0.5}O_4$ and Li-metal electrodes measured at 95 °C. The red dot line at 3.8 V indicates the theoretical prediction for decomposition reactions by Ceder *et al.*[31]

of the theoretical patterns (ICSD 182312[39]) and (ICSD 70023[40]), the composite cathode before cycling and the composite cathode after cycling are shown in Fig. 3. The sample for the composite cathode before cycling was directly taken from the dried cathode slurry, and the sample for the composite cathode after cycling was taken near the interface region by carefully scratching the material off the pellet after disassembly of the cell in an Ar-filled glove-box. Before battery operation all diffraction peaks can be matched with the theoretical patterns (ICSD 182312[39]) and (ICSD 70023[40]). After the battery operation, additional diffraction peaks belonging to neither c-$Li_{6.4}Ga_{0.2}La_3Zr_2O_{12}$ nor $LiMn_{1.5}Ni_{0.5}O_4$ are found in the XRD powder pattern of the composite cathode. The new occurring peaks at 2θ = ~18.6 and 44.8 degrees (indicated by a purple and pink diamond in Fig. 3) could correspond to the most intense diffraction peaks of the phases $(Li_{0.35}Ni_{0.05})NiO_2$ (ICSD 78704[41]) and Li_2MnO_3 (ICSD 165686[42]). However, the other less intense additional diffraction peaks (shown by small stars (*)) couldn't be clearly assigned to any binary compounds, educts or any predicted decomposition products of the electrolyte in the work of Ceder *et al.*[31] Nevertheless, the occurrence of additional new phases after the battery operation clearly confirms a decomposition reaction between the cathode material $LiMn_{1.5}Ni_{0.5}O_4$ and the solid electrolyte c-$Li_{6.4}Ga_{0.2}La_3Zr_2O_{12}$ during the first charging process. In addition, a right shift in the diffraction peaks of the solid elec-

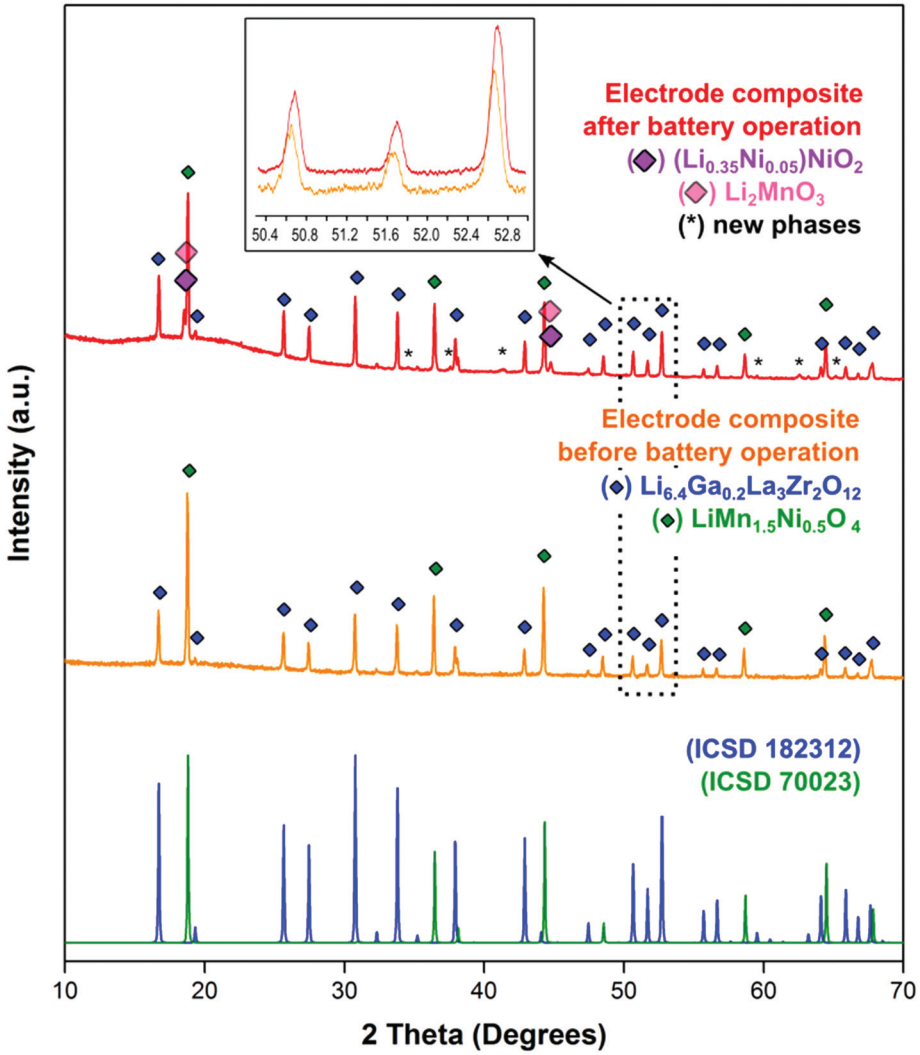

Fig. 3 Powder X-ray diffraction (XRD) pattern of $Li_{6.4}Ga_{0.2}La_3Zr_2O_{12}$ reference (blue) and $LiMn_{1.5}Ni_{0.5}O_4$ reference (green), electrode composite (c-$Li_{6.4}Ga_{0.2}La_3Zr_2O_{12}$, $LiMn_{1.5}Ni_{0.5}O_4$, conductive carbon and PVDF) before battery operation (orange) and electrode composite after battery operation (red).

trolyte c-$Li_{6.4}Ga_{0.2}La_3Zr_2O_{12}$ after the battery operation is found in the post-mortem XRD powder pattern, see Fig. 3. Such shifts in the pattern could indicate a Li-loss from the solid electrolyte that results in a reduction in the unit cell parameters. Besides, the decomposition reaction between the solid electrolyte and the cathode is predicted to be initiated by the Li uptake from the solid LLZO-garnet electrolyte. Consequently, we found that the cubic cell constant was 12.9907 Å (index with Werner's algorithm (TREOR)[43]) before the battery operation, see ESI Table 1,† whereas it was reduced to 12.9825 Å (index with Werner's algorithm (TREOR)[43]) after the battery operation, see ESI Table 2.† These findings clearly indicate a lithium loss from the c-$Li_{6.4}Ga_{0.2}La_3Zr_2O_{12}$ solid electrolyte during the first charging process.

To further probe the interface region between the composite cathode and the c-$Li_{6.4}Ga_{0.2}La_3Zr_2O_{12}$ solid electrolyte pellet after the battery operation, energy dispersive X-ray (EDX) spectra were obtained from the cross section of the cells. SEM micrograph and EDX spectra of the cell cross-section from the respective regions are displayed in Fig. 4 and ESI Fig. 5.† Indicated are six EDX probing spots denoted as spot 1 taken as the reference at the electrode, spots 2 and 3 taken at the cathode–electrolyte interfacial region and the spots 4–6 taken from far regions in the bulk of the solid electrolyte. The spectra from 3 to 6 reveal that no new phases containing the transition metal (Mn) can be found at the cathode–electrolyte interface at a distance of 10 μm from the electrode. Within the limits of this technique, it can be said that manganese of the cathode material does not diffuse into the solid electrolyte and does not contribute to the formation of new secondary phases deep into the solid electrolyte. However, in line with the findings from the post-mortem XRD powder patterns and electrochemical characterization, the lower intensities observed for the La and Zr peaks in spot 3 of the EDX obtained for the solid

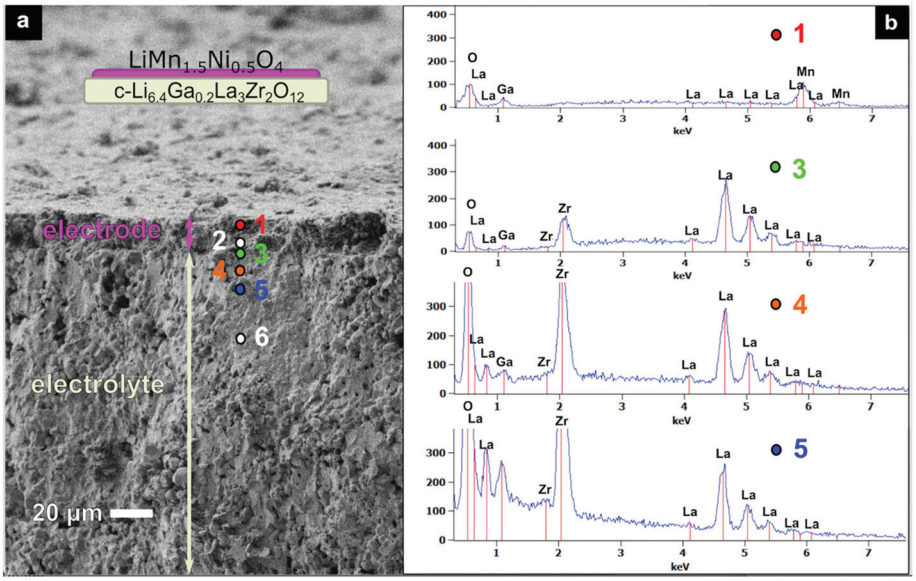

Fig. 4 (a) The cross section scanning electron microscopy (SEM) micrograph from an all-solid-state battery based on c-$Li_{6.4}Ga_{0.2}La_3Zr_2O_{12}$ and $LiMn_{1.5}Ni_{0.5}O_4$ electrodes obtained after the battery operation, displaying the solid electrolyte and the composite electrode. (b) Energy-dispersive X-ray spectroscopy (EDXS) data from the marked regions in (a) (for spectra of measurement points 2 and 6 see the ESI†).

electrolyte near to the interface-region again points to irreversible chemical reactions occurring between the solid electrolyte c-$Li_{6.4}Ga_{0.2}La_3Zr_2O_{12}$ and the electrode $LiMn_{1.5}Ni_{0.5}O_4$ upon the first charging process of the battery.

A model case representing all-solid-state batteries based on the garnet electrolyte c-$Li_{6.4}Ga_{0.2}La_3Zr_2O_{12}$ and the cathode material $LiMn_{1.5}Ni_{0.5}O_4$ after the battery operation is presented as schematic in Fig. 5. Through the experimental investigations, the post-mortem analysis carried out in this work and the theoretical investigations of Ceder *et al.*[31] the formation of new inactive phases in the interface region is considered to be initiated with the applied potential (at ~3.8 V) resulting in effective Li-loss from the solid electrolyte. The SEI (solid electrolyte interface) formation could normally block further reactions between the electrode and the electrolyte, but this is not the case here, as the irreversible reaction further continues and the cells cannot be cycled after the first charging process. The newly formed phases at the SEI are not electrochemically active under the given operation conditions; besides, the new interface region consisting of the new inactive phases and the Li-deficient garnet-type solid electrolyte could be expected to hamper the Li-ionic conductivity[23,44] and to further increase the interfacial resistance.[45] Based on the findings from this work, namely; (i) the potential drop at 3.8 V and the continuous irreversible reaction found in the first galvanostatic charge process, (ii) the formation of new phases during battery operation and (iii) the changes observed for the solid electrolyte c-$Li_{6.4}Ga_{0.2}La_3Zr_2O_{12}$ in post-mortem analysis; it can be stated that garnet type fast Li-ion conductors may not be suitable solid electrolytes for Li-ion batteries operating in combination with the cathode material $LiMn_{1.5}Ni_{0.5}O_4$ under given operations conditions (95 °C, 4.9–3.0 V potential window and *etc.*). The theoretical stability investigations on LLZO with respect to various cathodes and interfaces by the Ceder group[31] and Zhu *et al.*[32] are also thought to further support these points and raise the question if garnet-type solid electrolytes are in general suitable at high operation voltages above 3.8 V or may have to be operated at lower potentials. However, all-solid-batteries of garnets with alternative high voltage cathode materials (*e.g.* $LiNi_xMn_yCo_zO_2$ (NMC), $LiMnPO_4$, and *etc.*) should still be tested and investigated in real practical systems. In addition, the employment of protective interface layers that would limit the further reaction between the electrodes and the garnet-type solid electrolyte, and the tuning of valence and conduction bands of the solid electrolyte *via* alternative doping could be suggested as alternate ways for the stable operation of all-solid-state batteries based on garnet-type solid electrolytes. It should also be noted that garnet-type solid electrolytes could still enable the use of high capacity electrode materials, such as vanadate[4] and sulphur[5,6] based ones, as the operation of these cathode materials doesn't require relatively high voltage ranges.

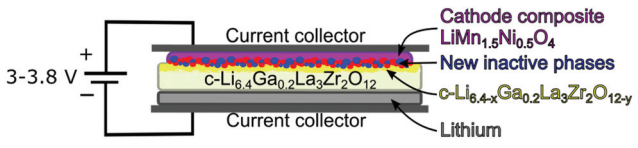

Fig. 5 Schematic representation of an all-solid-sate battery based on c-$Li_{6.4}Ga_{0.2}La_3Zr_2O_{12}$ with $LiMn_{1.5}Ni_{0.5}O_4$ and Li-metal electrodes with additional new phases and a lithium deficient c-$Li_{6.4-x}Ga_{0.2}La_3Zr_2O_{12-y}$ at the interface region of the electrolyte and cathode.

Conclusion

All-solid-state batteries based on the c-$Li_{6.4}Ga_{0.2}La_3Zr_2O_{12}$ (LLZO) solid electrolyte and $LiMn_{1.5}Ni_{0.5}O_4$ were successfully assembled *via* a simple and quick slurry deposition method which does not require any vacuum techniques. However, the galvanostatic cycling of batteries and the post-mortem analysis of the composite electrode before and after battery operation reveal that the solid electrolyte c-$Li_{6.4}Ga_{0.2}La_3Zr_2O_{12}$ is incompatible with the high-potential cathode material $LiMn_{1.5}Ni_{0.5}O_4$ within the limits of operation conditions. Despite the interface-design and pellet density, the battery cells crash during the first charging process indicated by a potential drop at around ~3.8 V and continuous irreversible reactions taking place at the electrolyte–electrode interface; *viz.* the discharging of the battery cells in the subsequent cycle is not possible. Post-mortem analysis of the all-solid-state batteries after the battery operation indicates the formation of new phases in the electrolyte–electrode interface region and a Li-loss from the solid electrolyte. These additional phases clearly prove that the cathode material and the solid electrolyte react at elevated working potentials. Our experimental findings are in line with theoretical stability calculations from the Ceder group[31] suspecting a limited chemical stability of LLZO in combination with various cathode materials starting at 3.8 V.

Through this work, we conclude that $LiMn_{1.5}Ni_{0.5}O_4$ as a cathode material may not be suitable in combination with the solid electrolyte c-$Li_{6.4}Ga_{0.2}La_3Zr_2O_{12}$ for all-solid-state batteries. Our experimental findings in combination with theoretical predictions raise the question if the garnet-type solid electrolyte LLZO is in general suitable for high-voltage cathode materials or if LLZO is just incompatible with $LiMn_{1.5}Ni_{0.5}O_4$ under given operation conditions.

Author contributions

Christian Hänsel and Semih Afyon should be considered co-first authors.

Acknowledgements

The authors thank Competence Center Energy and Mobility (CCEM) and ALSTOM for funding of the projects: Proposal 911 "All Solid State Li-Ion Batteries based on New Ceramic Li-Ion Electrolytes" and SP-ESC-A 03-14, ETH Zürich Foundation "All Solid State Li+ Batteries with high Thermal Operation Window", respectively.

References

1 J. M. Tarascon and M. Armand, *Nature*, 2001, **414**, 359–367.
2 P. G. Bruce, S. A. Freunberger, L. J. Hardwick and J. M. Tarascon, *Nat. Mater.*, 2012, **11**, 19.
3 C. M. Hayner, X. Zhao and H. H. Kung, *Annu. Rev. Chem. Biomol. Eng.*, 2012, **3**, 445–471.
4 S. Afyon, F. Krumeich, C. Mensing, A. Borgschulte and R. Nesper, *Sci. Rep.*, 2014, **4**, 7113.
5 X. Ji, K. T. Lee and L. F. Nazar, *Nat. Mater.*, 2009, **8**, 500–506.
6 J. Schuster, G. He, B. Mandlmeier, T. Yim, K. T. Lee, T. Bein and L. F. Nazar, *Angew. Chem., Int. Ed.*, 2012, **51**, 3591–3595.
7 P. Knauth, *Solid State Ionics*, 2009, **180**, 911–916.
8 C. Cao, Z.-B. Li, X.-L. Wang, X.-B. Zhao and W.-Q. Han, *Front. Energy Res.*, 2014, **2**, 1–10.
9 R. Murugan, V. Thangadurai and W. Weppner, *Angew. Chem., Int. Ed.*, 2007, **46**, 7778–7781.
10 E. J. Cussen, *J. Mater. Chem.*, 2010, **20**, 5167.
11 V. Thangadurai, S. Narayanan and D. Pinzaru, *Chem. Soc. Rev.*, 2014, **43**, 4714–4727.
12 C. A. Geiger, E. Alekseev, B. Lazic, M. Fisch, T. Armbruster, R. Langner, M. Fechtelkord, N. Kim, T. Pettke and W. Weppner, *Inorg. Chem.*, 2011, **50**, 1089–1097.
13 E. Rangasamy, J. Wolfenstine and J. Sakamoto, *Solid State Ionics*, 2012, **206**, 28.
14 Y. Jin and P. J. McGinn, *J. Power Sources*, 2011, **196**, 8683–8687.
15 W. G. Zeier, S. Zhou, B. Lopez-Bermudez, K. Page and B. C. Melot, *ACS Appl. Mater. Interfaces*, 2014, **6**, 10900–10907.
16 G. T. Hitz, E. D. Wachsman and V. Thangadurai, *J. Electrochem. Soc.*, 2013, **160**, A1248.
17 C. Bernuy-Lopez, W. Manalastas, J. M. del Amo, A. Aguadero, F. Aguesse and J. A. Kilner, *Chem. Mater.*, 2014, **26**, 3610.
18 R. Jalem, M. J. D. Rushton, W. Manalastas, M. Nakayama, T. Kasuga, J. A. Kilner and R. W. Grimes, *Chem. Mater.*, 2015, **27**, 2821–2831.
19 D. Rettenwander, J. Langer, W. Schmidt, C. Arrer, K. J. Harris, V. Terskikh, G. R. Goward, M. Wilkening and G. Amthauer, *Chem. Mater.*, 2015, **27**, 3135–3142.
20 D. Rettenwander, G. Redhammer, F. Preishuber-Pflugl, L. Cheng, L. Miara, R. Wagner, A. Welzl, E. Suard, M. M. Doeff, M. Wilkening, J. Fleig and G. Amthauer, *Chem. Mater.*, 2016, **28**, 2384–2392.
21 R. Wagner, G. J. Redhammer, D. Rettenwander, A. Senyshyn, W. Schmidt, M. Wilkening and G. Amthauer, *Chem. Mater.*, 2016, **28**, 1861–1871.
22 H. El Shinawi and J. Janek, *J. Power Sources*, 2013, **225**, 13–19.
23 S. Afyon, F. Krumeich and J. L. M. Rupp, *J. Mater. Chem. A*, 2015, **3**, 18636–18648.
24 J. Van den Broek, S. Afyon and J. L. M. Rupp, *Adv. Energy Mater.*, 2016, 1600736.
25 S. Ohta, J. Seki, Y. Yagi, Y. Kihira, T. Tani and T. Asaoka, *J. Power Sources*, 2014, **265**, 40–44.
26 S. Ohta, T. Kobayashi, J. Seki and T. Asaoka, *J. Power Sources*, 2012, **202**, 332–335.
27 S. Ohta, T. Kobayashi and T. Asaoka, *J. Power Sources*, 2011, **196**, 3342–3345.

28 S. Ohta, S. Komagata, J. Seki, T. Saeki, S. Morishita and T. Asaoka, *J. Power Sources*, 2013, **238**, 53–56.
29 T. Kato, T. Hamanaka, K. Yamamoto, T. Hirayama, F. Sagane, M. Motoyama and Y. Iriyama, *J. Power Sources*, 2014, **260**, 292–298.
30 M. Kotobuki, H. Munakata, K. Kanamura, Y. Sato and T. Yoshida, *J. Electrochem. Soc.*, 2010, **157**, A1076.
31 L. J. Miara, W. D. Richards, Y. E. Wang and G. Ceder, *Chem. Mater.*, 2015, **27**, 4040–4047.
32 Y. Zhu, X. He and Y. Mo, *J. Mater. Chem. A*, 2016, **4**, 3253.
33 J. H. Kim, N. P. Pieczonka and L. Yang, *ChemPhysChem*, 2014, **15**, 1940–1954.
34 H. Liu, J. Wang, X. Zhang, D. Zhou, X. Qi, B. Qiu, J. Fang, R. Kloepsch, G. Schumacher, Z. Liu and J. Li, *ACS Appl. Mater. Interfaces*, 2016, **8**, 4661–4675.
35 Z. Moorhead-Rosenberg, A. Huq, J. B. Goodenough and A. Manthiram, *Chem. Mater.*, 2015, **27**, 6934–6945.
36 A. Manthiram, K. Chemelewski and E.-S. Lee, *Energy Environ. Sci.*, 2014, **7**, 1339.
37 S. Bin Park, H. C. Shin, W.-G. Lee, W. Il Cho and H. Jang, *J. Power Sources*, 2008, **180**, 597–601.
38 D. Johnson, *ZView Software, 3.2c*, Scribner Associates, Inc., 2008.
39 J. Awaka, A. Takashima, K. Kataoka, N. Kijima, Y. Idemoto and J. Akimoto, *Chem. Lett.*, 2011, **40**, 60–62.
40 D. Gryffroy and R. E. Vandenberghe, *J. Phys. Chem. Solids*, 1992, **53**, 777–784.
41 A. Hirano, R. Kanno, Y. Kawamoto, Y. Takeda, K. Yamaura, M. Takano, K. Ohyama, M. Ohashi and Y. Yamaguchi, *Solid State Ionics*, 1995, **78**, 123.
42 A. Boulineau, L. Croguennec, C. Delmas and F. Weill, *Chem. Mater.*, 2009, **21**, 4216.
43 P. E. Werner, L. Eriksson and M. Westdahl, *J. Appl. Crystallogr.*, 1985, **18**, 367–370.
44 J. Wolfenstine, J. Ratchford, E. Rangasamy, J. Sakamoto and J. L. Allen, *Mater. Chem. Phys.*, 2012, **134**, 571–575.
45 A. C. Luntz, J. Voss and K. Reuter, *J. Phys. Chem. Lett.*, 2015, 4599–4604.

